Materials Today Bio 30 (2025) 101432

Contents lists available at ScienceDirect

Materials Today Bio

journal homepage: www.journals.elsevier.com/materials-today-bio

Enhanced hydrogel loading of quercetin-loaded hollow mesoporous cerium dioxide nanoparticles for skin flap survival

Xiangjun Liu [a], Yikun Ju [a], Pu Yang [a], Naisi Shen [a], Yunyuan Shao [b], Anqi Yang [a], Rui Wu [a], Lanjie Lei [b,*], Bairong Fang [a,**]

[a] Department of Plastic and Aesthetic (Burn) Surgery, The Second Xiangya Hospital, Central South University, Changsha, 410011, China
[b] Key Laboratory of Artificial Organs and Computational Medicine in Zhejiang Province, Institute of Translational Medicine, Zhejiang Shuren University, Hangzhou, 310015, China

ARTICLE INFO

Keywords:
Quercetin
Cerium dioxide
Skin flap
Oxidative stress

ABSTRACT

Flap techniques are indispensable in modern surgery because of their role in repairing tissue defects and restoring function. Ischemia-reperfusion and oxidative stress-induced injuries are the main causes of flap failure. Oxidative stress exacerbates cell damage through the accumulation of reactive oxygen species (ROS), thereby affecting flap function and survival. Effective management of these factors is essential for improving flap survival and post-operative recovery. In this study, we utilized hollow mesoporous cerium dioxide nanoparticles loaded with quercetin, which were later loaded into a light-cured double cross-linked hydrogel (HQu@BC) and injected into the flap site to activate macrophage reprogramming to maintain local ROS homeostasis and reduce inflammation. Quercetin scavenges ROS and reduces mitochondrial oxidative stress due to its intrinsic reducing structures such as catechols, carbon-carbon double bonds, and hydroxyl synergistic mesoporous cerium dioxide nanoparticles, and inhibits inflammation by suppressing M1 macrophage polarization. This system continuously regulates ROS levels, kills bacteria and ultimately reduces inflammation, thereby creating a favorable microenvironment for flap survival. This innovative injectable composite nanoparticle hydrogel material has anti-inflammatory, antioxidant, antimicrobial, and healing-promoting properties, providing a new approach to improving the success of flap surgery.

1. Introduction

With the acceleration of modern urbanization and popularization and use of modern mechanical technology, patients with skin- and tissue-defects account for an increasing proportion of emergency care patients. Additionally, diabetes, a major health problem in aging populations, has led to an increased number of patients with chronic skin defects [1]. Flap surgery vital in the surgical field, in which tissue flaps are used to repair traumatic injuries [2], congenital malformations [3], defects after tumor resection [4,5], burns [6], and other morphological and functional defects [7,8]. Flaps have a distinct therapeutic effect on skin defects and can greatly reduce the recovery time and treatment costs [9]. More importantly, flap surgery is also crucial in the field of reconstruction [10], as it can restore joint function and the appearance of vital organs (such as breast reconstruction [11], nasal reconstruction, and ear reconstruction [12]) and can help patients continue a normal life. However, failed flap surgery results in wounds or defects that need to be covered and may not heal effectively. This can prolong treatment durations and increase the risk of infection and other complications [13]. In addition, flap surgery failure may result in dysfunction or permanent damage if it affects vital organs or functional areas, such as the face, hands, and joints [14].

After flap transplantation, the original blood supply is cut off during the operation, and when the blood flow is restored after surgery, the tissues suffer from various stressors, such as hypoxia, nutrient deficiency, and accumulation of metabolic waste products, resulting in severe disruption of cell function and structure and irreversible necrosis of the flap [15]. This is partially due to a lack of oxygen in tissues during ischemia, which leads to mitochondrial dysfunction and increased oxygen radical production. During reperfusion, oxygen radicals are released in large quantities, causing oxidative stress-induced damage to cell membranes, proteins, and nucleic acids [16]. Ischemia-reperfusion

* Corresponding author.
** Corresponding author.
E-mail addresses: leilanjie1988@163.com (L. Lei), fbrfbr2004@csu.edu.cn (B. Fang).

https://doi.org/10.1016/j.mtbio.2024.101432
Received 5 November 2024; Received in revised form 6 December 2024; Accepted 26 December 2024
Available online 28 December 2024

injury leads to increased release of inflammatory mediators, such as tumor necrosis factor-α (TNF-α), interleukin-1β (IL-1β), and IL-6, exacerbating tissue damage [17], promoting vascular endothelial cell adhesion and thrombosis, and further affecting the blood and nutrient supply of the flap. Although advances in microvascular surgery and improved postoperative management have significantly reduced the risk of flap necrosis, these methods are limited by their requirements for high-cost equipment and experienced surgeons, therefore more effective strategies are needed to improve flap survival and functional recovery.

Quercetin (3,3′,4′,5,7-pentahydroxyflavone) is a flavanol that is widely found in fruits and vegetables, and humans typically consume around 5–40 mg per day [18]. However, the poor solubility of quercetin in water, its fast metabolism and short half-life in vivo limit its application. Its loading using nanomaterials with hollow mesoporous structure can enhance drug utilization and exert better therapeutic effects. Previous studies have found that cerium dioxide has antioxidant, anti-inflammatory and antimicrobial properties, which can act synergistically with quercetin [19]. Therefore, in the present study, it is proposed to use hollow mesoporous cerium dioxide ($HCeO_2$) for loading quercetin, to improve its stability and bioavailability and to exert stronger antioxidant and anti-inflammatory effects. In response to the overproduction of ROS and excessive inflammatory response during skin flap transplantation, we propose to load quercetin using HCeO2 and investigate its possible role in skin flap regeneration, focusing on its role in antioxidant and anti-inflammatory properties.

In this study, a hydrogel based on natural polymers was constructed for drug delivery, allowing the constructed composite nanoparticles to act locally on the skin flap (Fig. 1). In this study, chondroitin sulfate and bovine serum albumin (BSA) were chosen as the basic materials of the hydrogel, both of which are natural polymers with good biocompatibility and degradability [20,21]. Methacrylic acid-modified BSA (BSAMA) and oxidized chondroitin sulfate (OCS) can be crosslinked by Schiff base and light to form hydrogels, and the double crosslinking strategy improves the mechanical strength and stability of hydrogels. In addition, the controllable degree of cross-linking allows the physical properties of the hydrogel to be adjusted for different applications [22]. The composite hydrogel provides an ideal environment for the application of skin flaps, which can effectively improve the survival rate and healing effect of skin flaps. This carrier system not only helps to reduce the dose and frequency of drug administration but also improves treatment efficacy and reduces potential side effects, and these findings support the further development of quercetin for clinical applications.

2. Results and discussion

2.1. Characterization of Enhanced BC hydrogel

Previous studies found that the shape, structure, drug release, and hemolytic behavior of BSAMA at concentrations of 3 %, 5 %, and 10 % showed minimal changes after autoclaving [23]. In this study, we developed a BSA and CS-based hydrogel (BC hydrogel), specifically constructed from 8 % w/v BSAMA and 8 % w/v OCS by Schiff base reaction and photo-crosslinking. The aldehyde groups (-CHO) in OCS and the primary amines (-NH_2) in BSAMA forming imine (Schiff base)

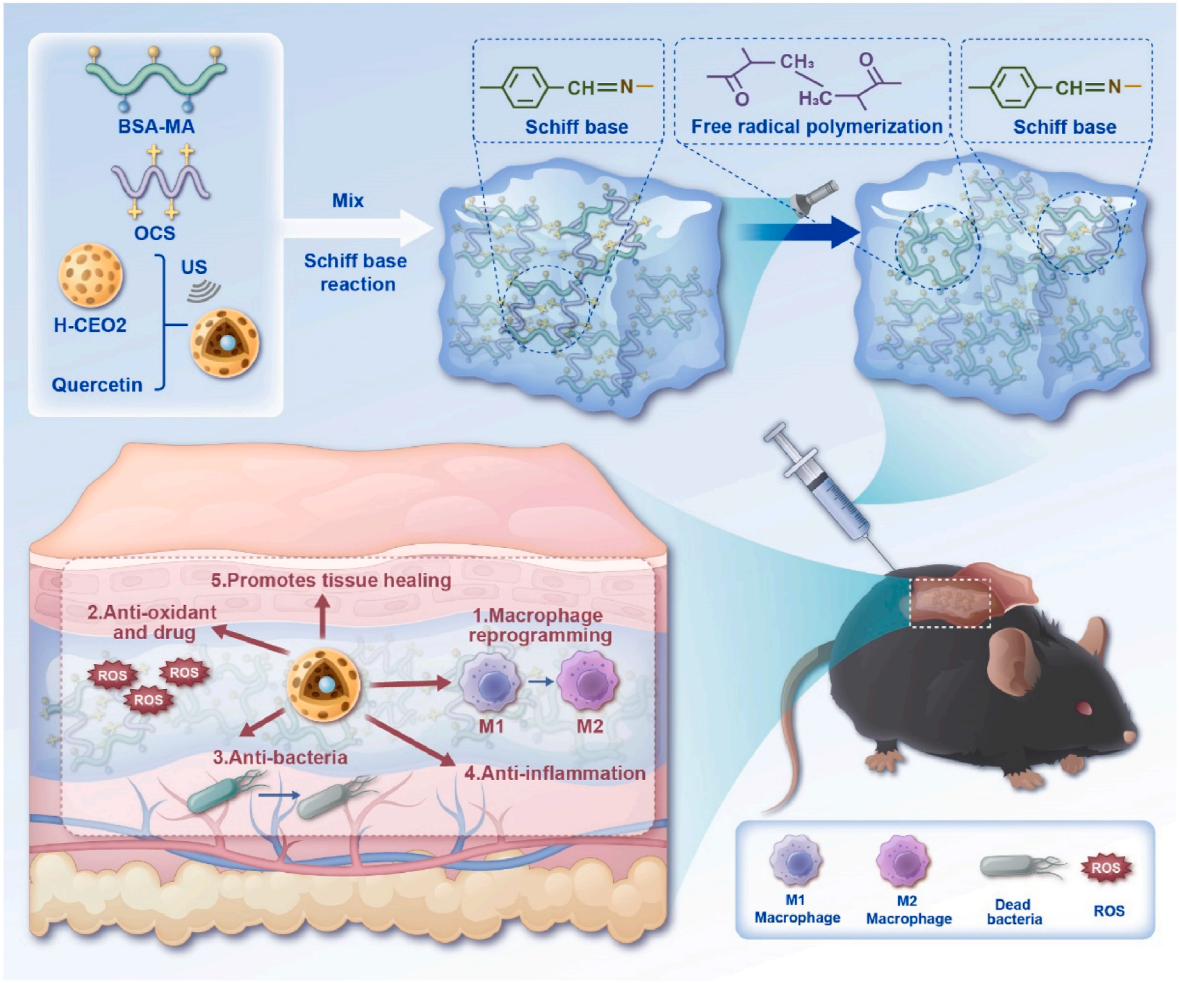

Fig. 1. Schematic showing the fabrication of HQu@BC hydrogel and its potential application in Subcutaneous of the flap.

through the Schiff base reaction. In the gelation process, we observed that the BSAMA and OCS solutions exhibited good fluidity at room-temperature. When these two solutions were mixed, their fluidity decreased and the internal structure changed, forming the precursor of single-network BC (pre-BC) (Fig. 2a). Subsequently, 3 min of UV irradiation significantly affected the structure and rheological properties of the solution, resulting in a photo-crosslinked dual-network BC hydrogel (Fig. 2a).

Before UV irradiation, the storage modulus (G′) and loss modulus (G″) of the pre-BC hydrogel were relatively low and showed little change. After UV irradiation, G′ of BC significantly increased, indicating enhanced elasticity, whereas G″ slightly increased, indicating increased viscosity (Fig. 2b). The viscosity of pre-BC decreased with increasing shear rate, whereas after UV irradiation, the viscosity of BC remained stable at high shear rates and was generally high (Fig. 2c). In summary, UV irradiation enhanced the storage modulus, loss modulus, and viscosity of BC, improving its mechanical strength, elasticity, and viscosity. The subsequent dynamic rheological experiments on the hydrogel showed that its mechanical properties remained stable at each time step, demonstrating good elasticity (Fig. 2d). These results indicate that the photocrosslinked dual-network BC hydrogel can better withstand external pressure or stretching, reducing the risk of rupture or deformation under the skin. In particular, the enhanced elasticity and viscosity are more conducive to the adhesion of the BC hydrogel to subcutaneous tissue, allowing it to adapt to the movement and deformation of subdermal tissues, thereby minimizing discomfort caused by displacement or deformation of the hydrogel.

The microstructural characteristics of the freeze-dried pre-BC and BC samples were characterized using SEM (Fig. 2e). SEM analysis revealed that the pre-BC hydrogel before UV irradiation had relatively large pore structures with a more uniform distribution. After UV irradiation, the BC hydrogels exhibited significantly different microstructures. The pore sizes were notably smaller, pore distribution became denser. The internal structure of the pores was more complex, with more micropores and connection points, making the overall structure more compact. Microstructural analysis indicated that UV irradiation increased the density and uniformity of the pore structure of the material. These improvements are likely related to the crosslinking reactions induced by UV irradiation, which result in better performance and stability for practical applications.

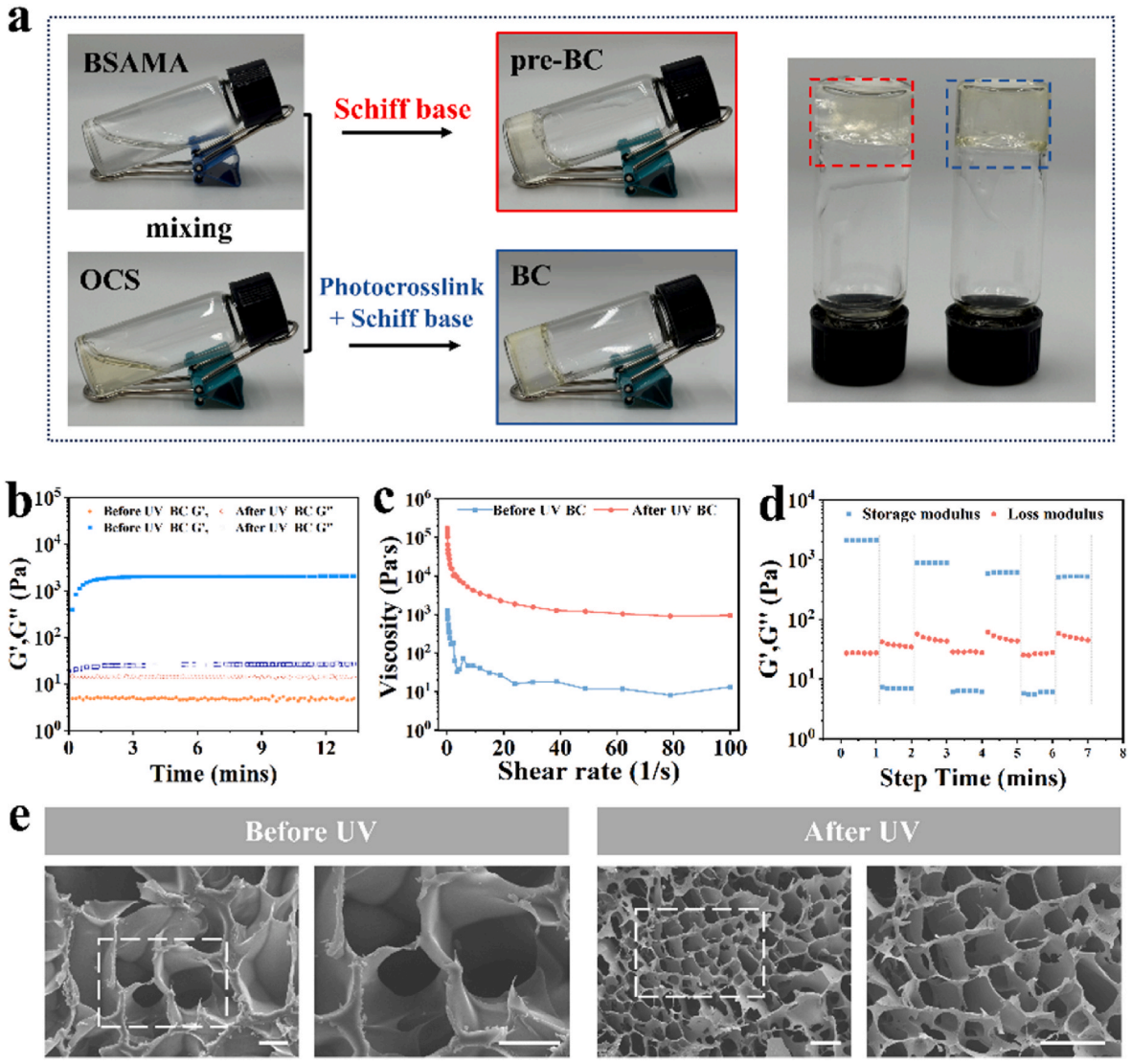

Fig. 2. Characterization of Enhanced BC Hydrogel (a) Vial tilt test. BSAMA and OCS can be initially formed into a hydrogel by Schiff base reaction (pre-BC), which can be photocrosslinked under UV light (BC) to further enhance its crosslinking degree. **(b)** Oscillation time sweep experiments. **(c)** Shear thinning experiment. **(d)** Alternating step strain sweep experiments. **(e)** Microstructures of pre-BC and BC hydrogels. scale bar: 50 μm.

2.2. Characterization of HCeO2 and Quercetin Composite Nanoparticles

We used transmission electron microscopy (TEM) to characterize the microstructure of HCeO2, revealed that HCeO2 nanoparticles were uniformly spherical with distinct hollow characteristics (Fig. 3a). These hollow structures and mesoporous properties enable the slow and sustained release of quercetin, helping maintain the effective concentration of the drug and reducing the frequency of administration. The energy dispersive X-ray spectroscopy (EDX) mapping images in Fig. 3b confirm the composition of the HCeO2 particles, and the selected area electron diffraction (SAED) images show clear diffraction rings that indicate their polycrystalline nature and specific interplanar spacings (Fig. 3c). These features indicate that the HCeO2 particles have a large specific surface area and pore volume, allowing them to load more quercetin molecules, thereby increasing the drug-loading capacity. Particle size distribution of hollow mesoporous cerium oxide nanoparticles was measured using a particle size analyzer. (Fig. 3d). The experimental results indicate that the particle size distribution of the hollow mesoporous cerium oxide nanoparticles follows a relatively normal distribution, with most particles having diameters centered around 150 nm. The size distribution primarily ranges between 100 nm and 200 nm. The histogram and fitted curve illustrate that the particle sizes are relatively uniform, suggesting good control over the nanoparticle size within the sample.

We constructed composite nanoparticles HCeO2@Qu (HQu) by loading quercetin into HCeO2 using physical adsorption. To evaluate their ability to scavenge ROS, we examined their SOD and CAT activities. The experimental results showed the scavenging activity of HQu against superoxide anion (O_2-) as well as free radical cation (·ABTS+) (Fig. 3e and f). The results showed that the increase in free radical scavenging was concentration dependent, which indicated that HQu possessed significant antioxidant activity. Both figures show that the scavenging activity increases with the concentration of HQu, indicating that the compound exhibits strong antioxidant effects. At the same time, we can visually observe that when HQu was added to the H_2O_2, a catalytic reaction took place and a large number of bubbles were produced, indicating its CAT activity (support Fig. 1).

2.3. The antibacterial efficacy of the HQu@BC hydrogel

The antibacterial effects of the blank control group and experimental groups on the growth of *Staphylococcus aureus (S. aureus)* and *Escherichia coli (E. coli)* were measured using the agar diffusion method. The antimicrobial results showed that the HQu group and HQu@BC group had better antimicrobial effects against both bacteria, and the number of bacterial colonies on the culture plates was significantly reduced (Fig. 4a). The results demonstrated that the number of colony-forming units (CFUs) in the HQu and HQu@BC groups was significantly lower than in the NC and BC groups, indicating strong antibacterial activity in both treatments (Fig. 4b and c). Bacterial live-dead staining showed the same results, with green representing living bacteria and red dead bacteria, and all groups containing HQu had better antibacterial effects (Fig. 4d, e, f). We used scanning electron microscopy to observe the treated bacteria in each group after fixation, and the electron microscope images of the bacteria showed that the bacteria in the NC group maintained a normal morphology, while the bacteria in the BC group appeared to be slightly aggregated (Fig. 4g). In contrast, bacteria in the HQu and HQu@BC groups displayed significant surface damage, further confirming the potent antibacterial effects of HQu@BC. These characteristics make HQu@BC highly suitable for preventing infections after flap surgery and improving postoperative healing outcomes.

2.4. Hemocompatibility, cytocompatibility, and organ toxicity

Considering that the hydrogels need to be placed subcutaneously in animal experiments, their biocompatibility needs to be examined. The blood compatibility of the hydrogels was investigated by hemolysis experiments. The hemolysis values of BC, HQu and HQu@BC were below the standard safety limit of 5 % (support Fig. 2). We selected

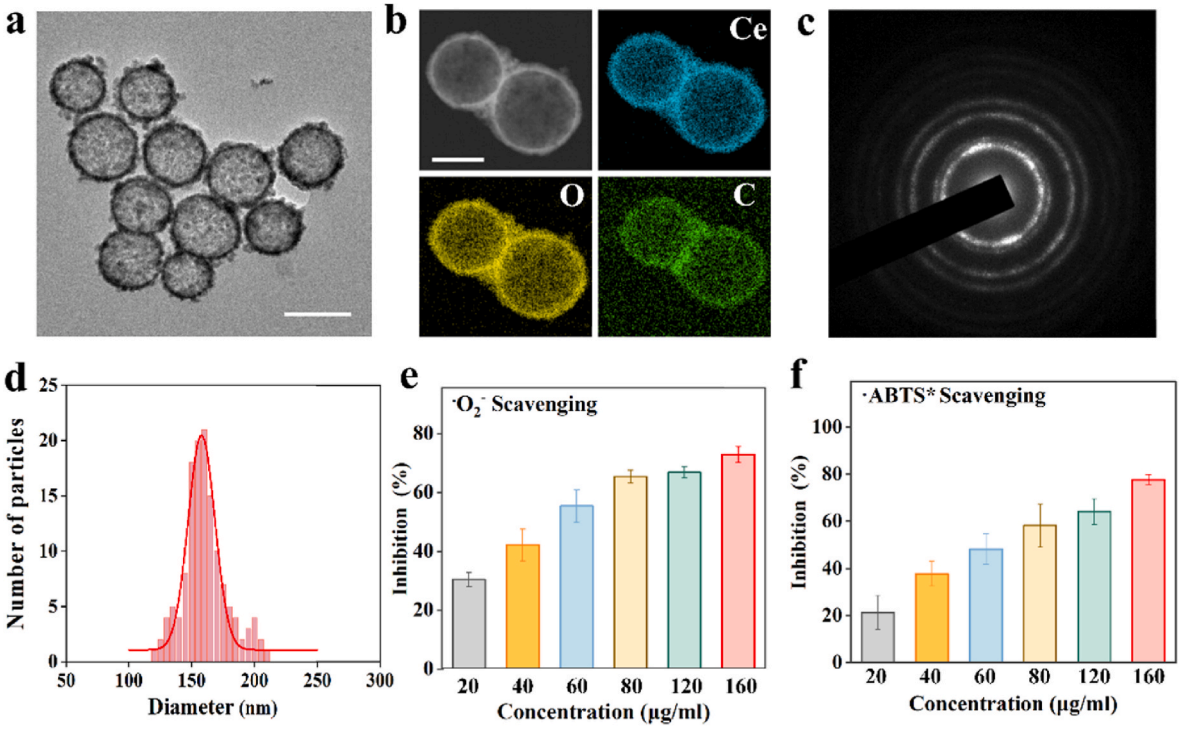

Fig. 3. Characterization of HCeO2 and Quercetin Composite Nanoparticles (a) TEM image of the topography of the hollow cerium dioxide particles. scale bar: 200 μm **(b)** EDX mapping image. The upper left image shows the TEM image of the hollow cerium dioxide particles, and the upper right, lower left, and lower right images are mapped images of different elements. Yellow, green, and blue correspond to the distribution of oxygen, cerium, and Carbon, respectively. scale bar:100 μm **(c)** SAED image showing the crystal structure of hollow cerium dioxide. **(d)** Particle size analysis of $HCeO_2$. **(e)** O_2^- **(f)** ·ABTS + scavenging ability of HQu.

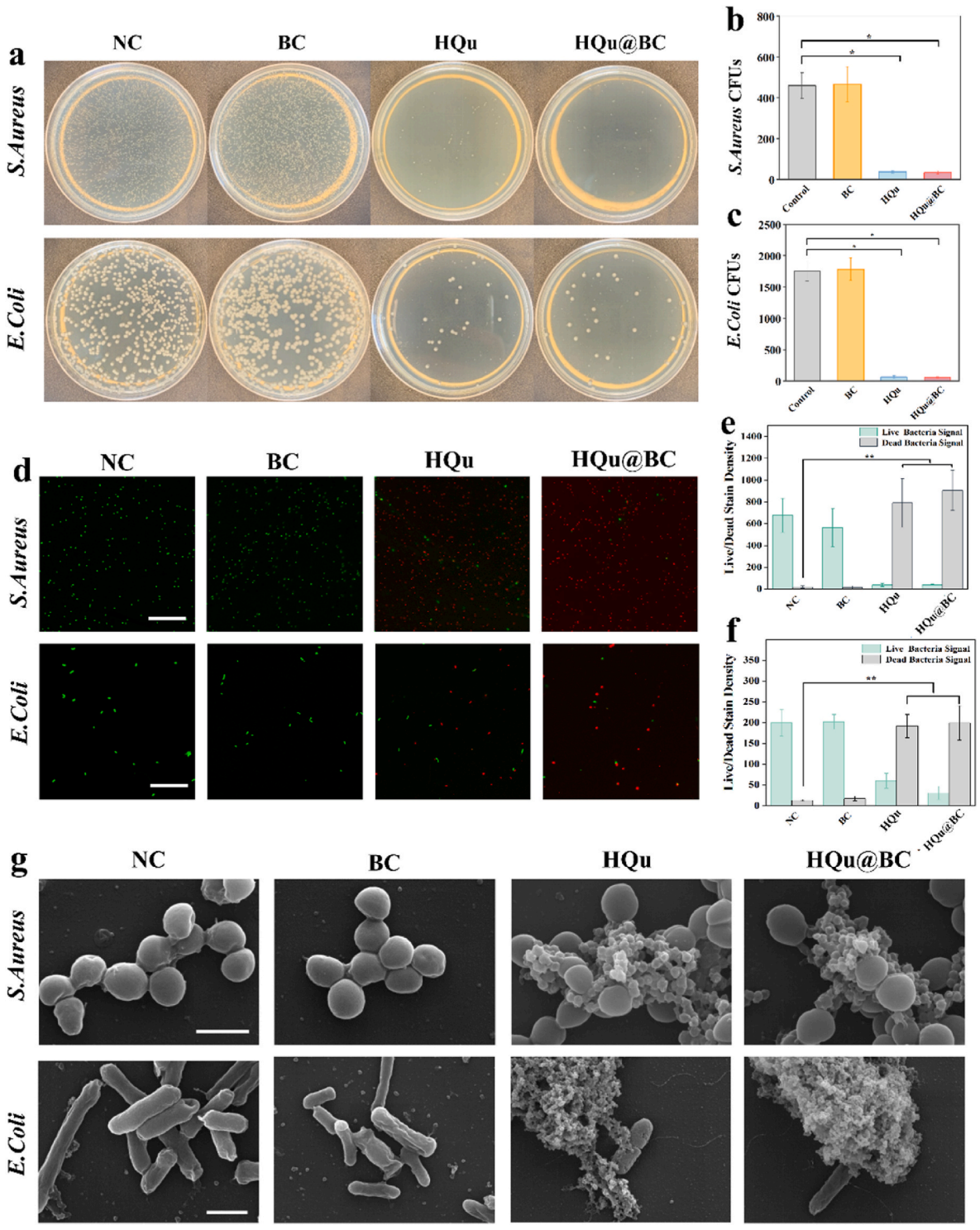

Fig. 4. Antibacterial activity of HQu@BC hydrogel. (a) The antibacterial activity of HQu@BC hydrogel against *S. aureus* and *E. coli* was determined using the agar diffusion method. **(b)** CFU counts of *S. aureus* and **(c)** *E. coli* after treatment. **(d)** Live-Dead Staining of *S. aureus* and *E. coli*. scale bar: 500 nm. **(e)** Fluorescence density of live/dead staining of *S. aureus*, and **(f)** *E. coli* treated with different solutions. **(g)** Morphological changes of bacteria treated with different solutions under electron microscopy. scale bar: 1 μm *P < 0.05, **P < 0.01.

human umbilical vein endothelial cells (HUVEC) to assess their cyto-compatibility. To investigate the effects of different concentrations of HQu on cell viability, the CCK-8 assay was used. The results showed that the cell viability of the HQu treatment group remained close to 100 % at concentrations of 0–160 μg/ml HQu, with almost no significant change (support Fig. 3). These results indicated that HQu had no significant effect on HUVEC viability in this concentration range, and its activity was not significantly affected. Afterwards, the cellular viability of HUVEC was further evaluated by live-dead cell staining and CCK8 assay after 24 h of incubation using hydrogel leachate. The results showed that there was no significant difference in cell viability between the groups. (Fig. 5a).

Visceral tissue samples obtained from mice that were subcutaneously injected with the HQu@BC hydrogel or saline were evaluated for

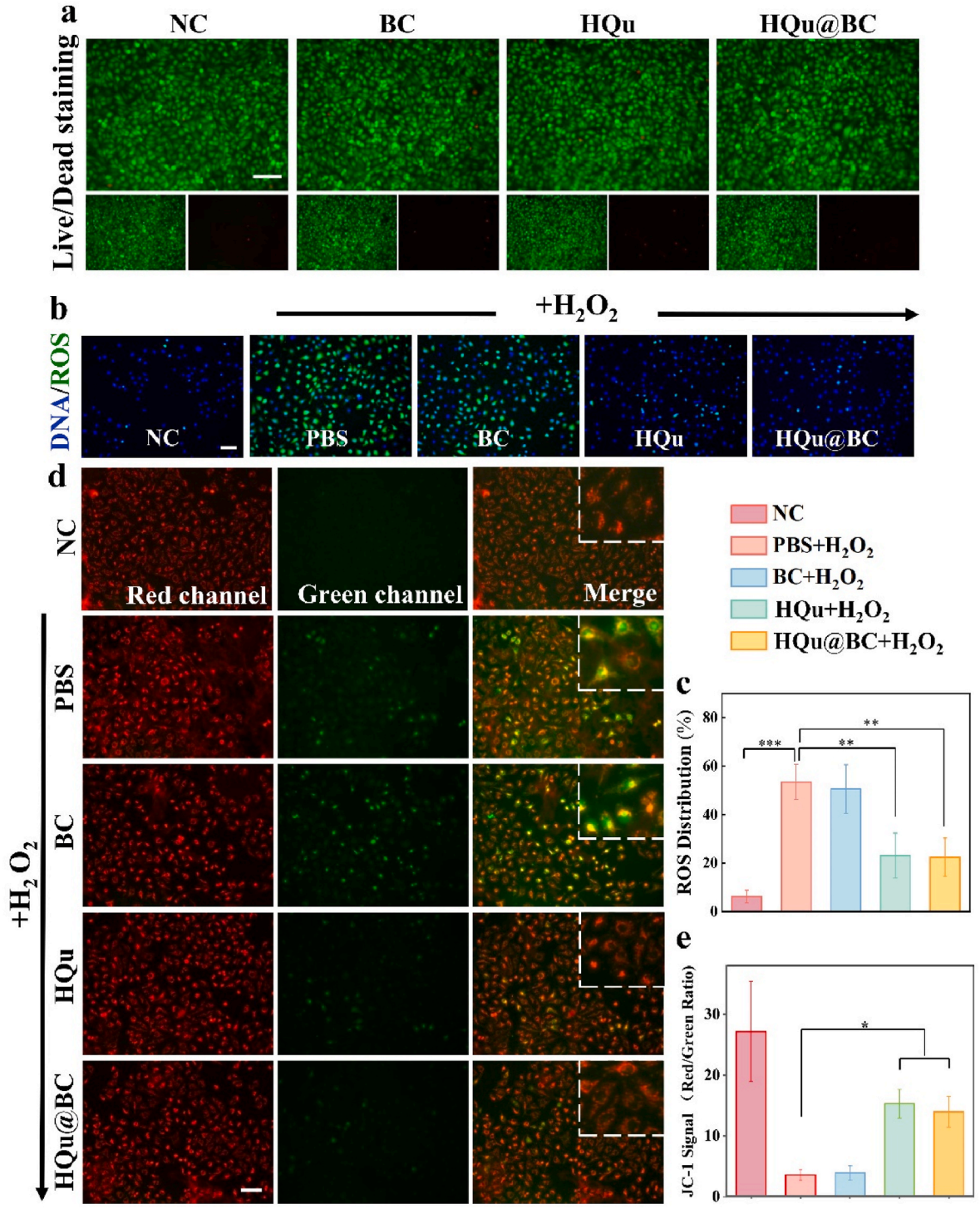

Fig. 5. Biocompatibility of HQu@BC hydrogel and its effects on ROS levels and mitochondrial function in HUVECs. (a) Live/dead staining of HUVECs after co-culture with hydrogel leachate. Scale bar = 100 μm. **(b)** Representative images of DCFH-DA fluorescence (green) showing ROS levels in the negative control, treated groups, and H_2O_2 group. Scale bar = 100 μm. **(c)** Relative fluorescence intensity quantification of ROS signals in different groups. **(d)** Mitochondrial membrane potential (MMP, ΔΨm) was detected by JC-1 staining in each group (red, high ΔΨm; green, low ΔΨm). Scale bar = 100 μm. **(e)** The ratio of red to green fluorescence intensity in each group. *P < 0.05, **P < 0.01, and ***P < 0.001.

potential pathological changes using HE staining. There were no significant differences in the morphology of the heart, liver, spleen, lungs, or kidney sections between the control and experimental mice (support Fig. 4). This means that the implantation of the HQu@BC hydrogel does not cause significant changes or damage to internal organs after 8 days or acute organ damage and has good biocompatibility.

2.5. HQu@BC reduces ROS levels and helps restore mitochondrial function in endothelial cells In vitro

Oxidative stress caused by elevated ROS levels can lead to damage in proteins, nucleic acids, and even trigger programmed cell death. Superoxide anions, hydrogen peroxide, and hydroxyl radicals are the main ROS involved in ischemia-reperfusion (I/R) injury. Reducing ROS levels

in endothelial cells could be an effective target to inhibit programmed cell death, while also providing some protection for tissue blood supply [18], which is beneficial under I/R conditions after flap surgery.

To investigate the antioxidant protective ability of HQu@BC on endothelial cells, intracellular ROS levels were measured using DCFH-DA (Fig. 5b and c). The results showed that compared to the NC group, the ROS fluorescence intensity was significantly increased in the PC group, indicating heightened oxidative stress in endothelial cells after H_2O_2 treatment. In contrast, HQu treatment significantly reduced ROS levels in endothelial cells, suggesting that HQu can effectively lower ROS levels in endothelial cells.

Mitochondria are one of the primary sources of ROS during I/R [23]. During ischemia, the electron transport chain (ETC) is impaired due to insufficient oxygen supply, leading to the accumulation of electrons. Upon reperfusion, the sudden restoration of oxygen causes an excessive transfer of these accumulated electrons to oxygen, producing large amounts of ROS (mainly superoxide anions, O_2^-). Oxidative stress damages mitochondrial DNA (mtDNA), proteins, and lipids, further impairing mitochondrial function and increasing ROS production, creating a vicious cycle. Therefore, we further explored the effects of HQu@BC on mitochondrial function.

The negative potential across the mitochondrial inner membrane, established by the proton pumps, is crucial for ATP production and the inhibition of cytochrome C release, serving as an indicator of mitochondrial integrity. The mitochondrial membrane potential (MMP), also known as ΔΨm, in healthy mitochondria, is reflected by the formation of aggregates that emit red fluorescence. Conversely, when MMP decreases, the dye remains in its monomer form, emitting green fluorescence. This red-to-green fluorescence shift is a direct indicator of MMP decline. Thus, the relative ratio of red to green fluorescence intensity can quantify the extent of mitochondrial depolarization. The MMP index of endothelial cells treated with hydrogen peroxide was significantly lower than that of the control cells (Fig. 5d and e), indicating impaired mitochondrial function following oxidative stress. Remarkably, HQu and HQu@BC application partially restored mitochondrial function.

2.6. Macrophage reprogramming in vitro

Macrophages can enhance flap survival through various mechanisms such as regulating inflammation, promoting angiogenesis, clearing apoptotic cells, and remodeling tissue. M2 macrophages not only exert anti-inflammatory effects and clear apoptotic cells but also remove harmful substances from the local environment, promote tissue repair, and secrete growth factors, particularly vascular endothelial growth factor (VEGF), to promote neovascularization, improve blood supply to the flap, and enhance flap survival. Upon exposure to pro-inflammatory stimuli (e.g., LPS, interferon-γ), macrophages are polarized toward the M1 phenotype, characterized by high expression of inducible nitric oxide synthase (iNOS), a major phenotype leading to inflammation. In contrast, CD206, also known as mannose receptor type C 1 (MRC1), is one of the markers of M2 macrophages, which is highly expressed in anti-inflammatory and tissue repair settings and has a positive effect on tissue repair and inhibition of excessive inflammation.

Therefore, we performed fluorescent staining for CD206 and iNOS and measured their expression levels in RAW264.7 cells under different treatment conditions to assess the effect of HQu on macrophage polarization. After treating macrophages with 1 μg/ml LPS, the positive control (PC) group showed stronger iNOS fluorescence signals than the normal control (NC) group, suggesting that the PC group successfully induced M1 macrophages. In the LPS + HQu group and the LPS + HQu@BC group, CD206 expression was significantly up-regulated, indicating that HQu inhibited macrophage polarization toward the M1 phenotype, and at the same time promoted the up-regulation of the M2 phenotype, thus exerting anti-inflammatory and tissue repair effects (Fig. 6a–c).

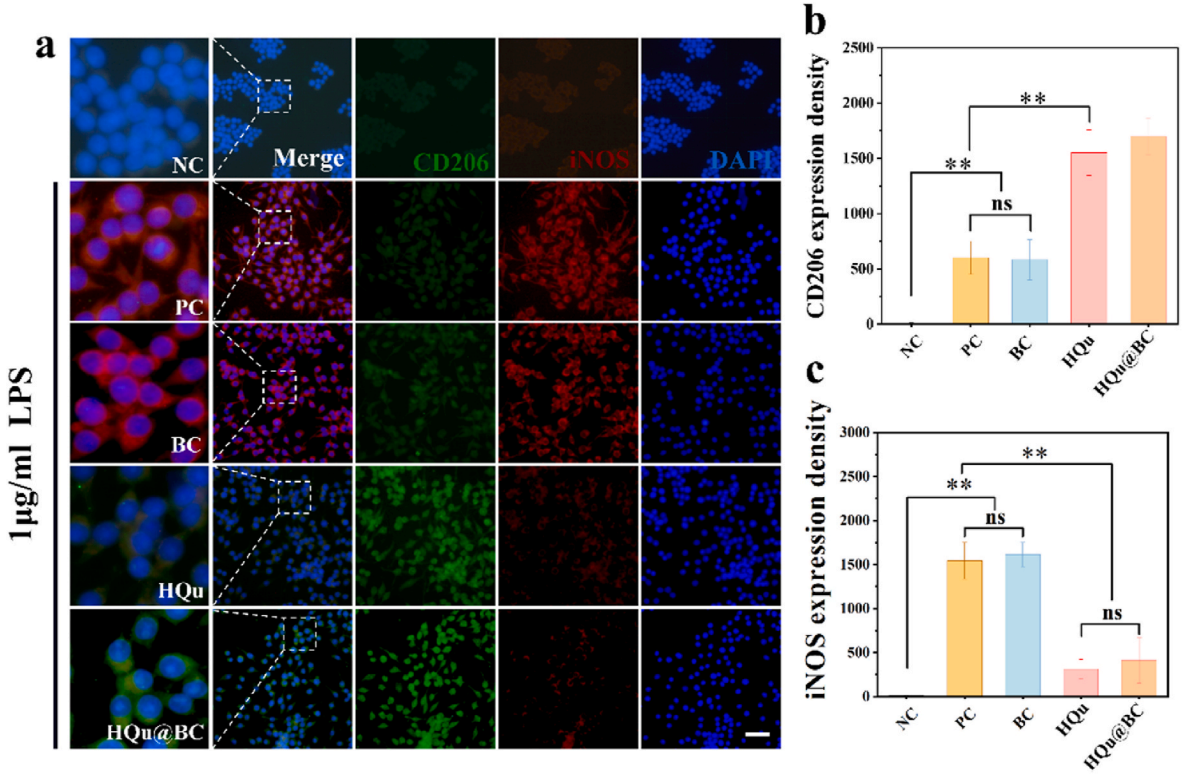

Fig. 6. Responses of macrophages on various samples *in vitro*. (a) Representative images of CD206, iNOS, and nucleic fluorescence staining of macrophages on various samples. **(b, c)** Analysis of fluorescence intensity of CD206 and iNOS of macrophages on various samples; Scale bar = 100 μm *P < 0.05, **P < 0.01.

2.7. Assessment of hydrogel-facilitated flap survival in vivo

We established a 10 × 30-mm mouse flap model. The control group was injected with saline under the flap, and the remaining groups were injected with BC hydrogel, HQu aqueous solution, and HQu@BC hydrogel, respectively. After injection, the edges of the flap were sutured, and the flap was photographed on days 0, 2, 4, 6, and 8 after the mouse flap model was established. The results showed that both the NC and BC groups showed obvious necrosis on day 8, with flaps displaying a darker color and a larger necrotic area (Fig. 7a). In contrast, flap necrosis was significantly reduced in the HQu and HQu@BC groups, particularly in the HQu@BC group, which had the smallest necrotic area and better skin color (Fig. 7b). This observation was further supported by the HE staining results (Fig. 7c), where the NC and BC groups showed severe tissue structure destruction and inflammatory cell infiltration, whereas the HQu and HQu@BC groups had mostly intact tissue structures and reduced inflammatory cell infiltration, especially in the HQu@BC group, where the tissue hierarchy was clear and there was almost no inflammatory cell infiltration. The results of immunohistochemical staining showed that IL-6 and TNF-α expression was higher in the NC and BC groups, and the stain color was dark brown, indicating a strong inflammatory response (Fig. 7d). However, the expression of IL-6 and TNF-α was significantly reduced in the HQu and HQu@BC groups, particularly in the HQu@BC group, where there was almost no obvious staining, and the inflammatory response was the mildest (Fig. 7e and f). These results suggest that the HQu@BC treatments can effectively promote flap survival, reduce the necrotic area, and significantly reduce inflammatory responses, especially HQu@BC, which has significant anti-inflammatory and health-promoting effects.

3. Materials and methods

3.1. Preparation of BC hydrogels

Bovine serum albumin (BSA) was dissolved in 0.25 M carbonate-bicarbonate buffer at 10 % (w/v), pH adjusted to 9.4. Methacrylic

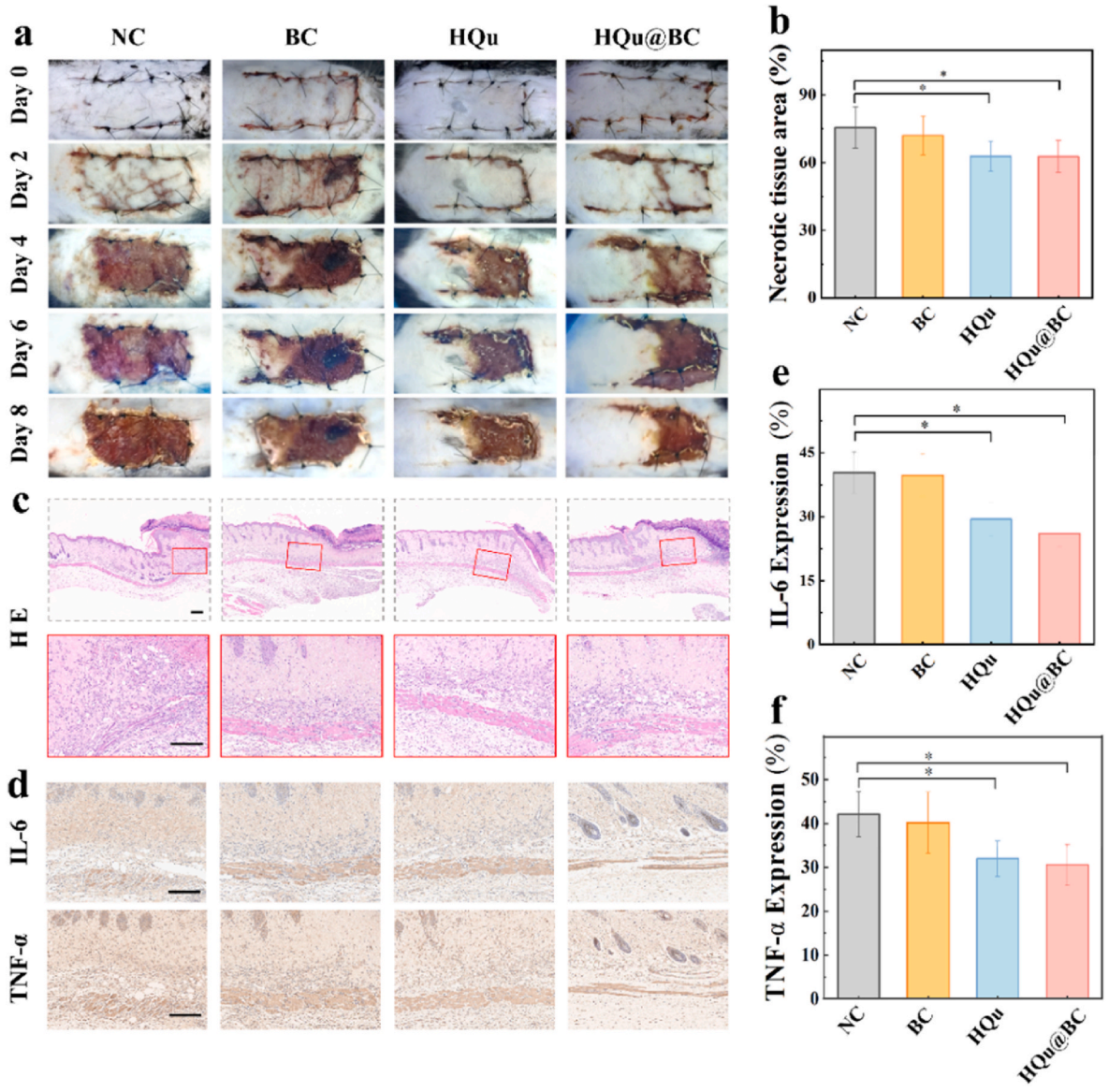

Fig. 7. Images of flap survival area and immunohistochemical images. (a) 0, 2, 4, 6 and 8 days after surgery, the survival area of mouse flaps **(b)** Comparison of each group's percentage of skin flap survival zones. **(c)** On the eighth day after surgery, the histopathology of the flap was evaluated under a light microscope following eosin (H&E) staining. Scale bar = 300 μm. **(d)** The expression level of IL-6 and TNF-α in flap tissue was assessed by immunohistochemistry on the 8th day after operation. Scale bar = 200 μm. **(e, f)** Analysis of expression of IL-6 and TNF-α of flap on various groups. *P < 0.05.

acid (MA) was added at a 1:2.2 M ratio to the free amino groups, and the mixture was stirred at 500 rpm for 1–2 h at 37 °C. After adjusting the pH to 7.4 to stop the reaction, the solution was filtered and dialyzed at 37 °C to remove unreacted MA and by-products. After lyophilization, BSAMA was stored at −20 °C for later use.

An aqueous solution of 2 % chondroitin sulfate was reacted with sodium periodate for 6 h. The reaction was stopped by adding ethylene glycol. After dissolving sodium chloride and absolute ethanol in a 1:2 vol ratio, a flocculent precipitate was formed and filtered to obtain a white product. The product was dissolved in 50 mL water and dialyzed in a dialysis bag (MWCO 8000–14,000) at 4 °C for 3–5 days, with water changes 2–3 times daily. The product was freeze-dried to yield chondroitin oxide sulfate (OCS) for storage.

3.2. Preparation of HQu

For the synthesis of HQu, HCeO2 was purchased from XFNANO Institute, and quercetin was purchased from MedChemExpress (MCE). Quercetin dissolved in DMSO, was slowly added dropwise to the aqueous HCeO2 solution, the solution was sonicated for 30 min in a 50 Hz ultrasonic cleaner and stirred at a constant speed for 24 h at 4 °C in the dark to ensure that the quercetin was sufficiently adsorbed into the pores of mesoporous cerium dioxide. The quercetin-loaded HCeO2 particles were dried at low temperature to obtain HQu.

3.3. Nanozyme activity analysis

The nanozyme activity of HQu was measured by determining superoxide dismutase (SOD) and catalase (CAT) activities. First, HQu nanoparticles were suspended in deionized water at concentrations of 0, 5, 10, 20, 40, 80, and 160 μg/mL for SOD activity measurements. The sample suspensions were then prepared according to the instructions of the total SOD assay kit. The SOD activity was calculated based on the absorbance change of water-soluble formazan dye at 560 nm, using the formula provided in the kit to determine the inhibition percentage of superoxide radicals ($O^{2\bullet-}$).

3.4. In vitro antimicrobial activity

The antimicrobial activity of HQu@BC composite hydrogel against Staphylococcus aureus and *Escherichia coli* was evaluated using the agar diffusion method and live/dead staining assay. A specific amount of bacterial in cryoprotectant solution was added to sterilized peptone medium and incubated overnight at 37 °C with shaking at 200 rpm. The bacterial cells were subcultured three times and then used for subsequent experiments. The bacteria were co-cultured with BC extract, HQu solution, or HQu@BC extract for 4 h. Subsequently, the bacterial suspension was diluted 100,000 times, and a plate coating assay was performed. After incubation at 37 °C for 16 h, photographs were taken to count the number of bacterial colonies. Additionally, a staining solution consisting of 1 μL of stain for every 100 μL of bacterial suspension was prepared. The bacterial samples were stained and incubated for 20 min at 37 °C, followed by imaging under a fluorescence microscope. Finally, bacterial specimens were fixed in 2.5 % glutaraldehyde for 12 h, dehydrated through an ethanol gradient, sputter-coated with gold, and examined using scanning electron microscopy (SEM). All hydrogel samples used in the experiments were sterilized by ultraviolet irradiation.

3.5. Cell culture and animal models

RAW264.7 cells were cultured in DMEM (Gibco, Life Technologies, China) supplemented with 10 % fetal bovine serum (FBS), 1 % penicillin-streptomycin. HUVECs were cultured in DMEM/F-12 medium supplemented with 10 % fetal bovine serum (FBS) and 1 % penicillin-streptomycin. All cells were grown in a humidified incubator at 37 °C with 5 % CO_2. Six-week-old male C57BL/6 mice (6-weeks-old, 20–22 g) were purchased from Slack Jingda Laboratory Animal Co. Ltd. Animals were housed in a controlled environment rearing room (temperature: 25 ± 1 °C, relative humidity: 50 ± 5 %, 12 h dark/light cycle from 6:00 a.m. to 6:00 p.m.) with free access to sterilized tap water and commercial laboratory rodent feed. All animal experiments were performed in accordance with the standards stipulated by the Chinese National Regulations for the Breeding and Use of Laboratory Animals. Animal experiments in this study were approved by the Animal Care and Use Committee of the Second Xiangya Hospital. (Approval No. 20241006).

3.6. In vitro toxicity assays

To evaluate the biocompatibility of HQu *in vitro*, HUVECs were seeded in 96-well microplates (1 × 104 cells/well) and cultured to 50%–80 % confluency. Different concentrations of HQu (0, 5, 10, 20, 40, 80, and 160 μg/mL) was then added to the cell culture medium in the 96-well plate and incubated. After 6 h, the cells were washed with PBS, and 100 μL of medium containing CCK-8 reagent was added and incubated for 2h. After 2 h of incubation, the optical density (OD) of each well was measured at 450 nm using a microplate reader. The absorbance data of each well were recorded, and cell viability was calculated. HUVEC survival was used to evaluate the cytotoxicity of HQu and BC hydrogels *in vitro*. Different groups of hydrogels were soaked in serum-free DMEM at 4 °C for 7 days and filtered using a 0.22 μm filter to obtain the corresponding leachates. All cell experiments described below were performed using leachates. Subsequently, the cells were treated under different conditions and were divided into blank control, BC hydrogel leaching solution, HQu, and HQu@BC hydrogel leaching solution groups. After the completion of each treatment, the medium was discarded, and the cells were gently washed twice with PBS. Next, an appropriate amount of live-dead dye mixture was added to each well (e.g., 100 μL per well) and incubated in a 37 °C, 5 % CO_2 incubator for 30–60 min (depending on the dye instructions). After incubation, the cells were gently washed twice with PBS to remove unbound dye. Next, the staining results were observed using a fluorescence microscope, with Calcein AM green fluorescence indicating live cells and PI red fluorescence indicating dead cells.

3.7. In vitro oxidative stress regulation

To assess the response of HUVECs treated with HQu@BC composite hydrogel under oxidative stress conditions, HUVECs were first seeded at an appropriate density in 24-well plates and cultured in a 37 °C, 5 % CO_2 incubator until they were 80 % confluent. The, the cells were gently washed twice with PBS for subsequent experiments. Cells were divided into five experimental groups: the control group (no treatment), the experimental group (treated with hydrogen peroxide alone at 800 μmol/L), and the hydrogel experimental group (treated with hydrogen peroxide followed by HQu and BC or HQu@BC leachate), and all cells were cultured in the incubator for 24 h. After incubation, the medium was removed from each well, and cells were treated with 10 μmol/L of DCFH-DA solution and an appropriate concentration of Hoechst 33342 staining solution. Then, the cells are further incubated for 30 min to allow DCFH-DA and Hoechst 33342 to fully penetrate and accumulate within the cells. Finally, the treated cells were observed and analyzed using fluorescence microscopy.

3.8. Mitochondrial observation

Mitochondrial membrane potential (MMP) was assessed using the JC-1 Assay Kit (Beyotime Institute of Biotechnology). HUVEC cells were seeded in 6-well plates and divided into five groups: negative control (NC), positive control (PC), BC, HQu, and HQu@BC. When the cells reached 80 % confluence, groups were treated with PBS or the respective solutions for 12 h. The NC and PC groups received equal volumes of PBS,

while the HQu group was treated with HQu solution, and the BC and HQu@BC groups received HQu@BC extract. After 12 h, treatment solutions were removed, and cells were washed with PBS. All groups except NC were then treated with hydrogen peroxide for 2 h. Following this, cells were washed again, and a JC-1 dye solution (10 μg/mL) was added for 30 min. After staining, cells were washed three times and observed under an inverted fluorescence microscope for analysis.

3.9. Immunofluorescence staining of macrophages (CD206 and iNOS)

RAW264.7 cells were seeded in cell crawlers in 12-well plates (2×10^6 cells/well), and cells were cultured at 37 °C until they reached approximately 50%–80 % confluency, and the compound wells were divided into five groups, in which the medium was replaced with DMEM complete culture medium (NC group), culture medium containing 1 μg/ml LPS (Sigma, L2880) (PC group), culture medium containing 1 μg/ml LPS + BC (LPS BC group), culture medium containing 1 μg/ml LPS + HQu (LPS HQu group), and culture medium containing 1 μg/ml LPS + HQu@BC (LPS HQu@BC group) for 12 h. The medium was carefully aspirated, and the cells were washed three times with PBS. Cells were fixed with 4 % paraformaldehyde for 15 min at 4 °C and then washed with PBS. After washing, the cells were permeabilized with 0.2 % Triton X-100 for 10 min and washed again with PBS. After washing, the cells were incubated at room temperature in 5 % BSA for 1 h. CoraLite® Plus 488-conjugated CD206 Polyclonal antibody and CoraLite®594-conjugated iNOS Polyclonal antibody (1:100, Proteintech Group, Inc) were diluted in 1 % BSA in PBS. The antibody solution was added to the cells and incubated overnight at 4 °C. Finally, the nuclei were detected using DAPI staining. Fluorescent images were captured using a Nikon confocal laser microscope (Nikon, A1 PLUS, Tokyo, Japan).

3.10. Establishment of the mouse flap model

In this experiment, 32 healthy male C57BL/6 mice were randomly assigned to four groups: the control, BC, HQu, and HQu@BC groups, with eight mice in each group. Before the experiment, the mice were anesthetized with inhaled isoflurane, and 10 × 30 mm dorsal flap separation surgery was performed. The control group was not administered the hydrogel, the BC and HQu@BC groups were administered the hydrogel under the skin flap, and the HQu group was injected with an equal volume of the HQu solution. Each flap was sutured with 5-0 nylon threads, spaced 5–10 mm apart.

The postoperative assessment of flap healing included skin color, texture, flexibility, and necrosis. The criteria for necrosis were grayish-black skin, atrophy, and loss of elasticity. On the 2nd, 4th, 6th, and 8th days after surgery, the mice were photographed under anesthesia, and the growth and viability of the flap were recorded. On the 8th postoperative day, the percentage of the necrotic area was calculated using the ImageJ software (necrotic area ÷ total flap area) × 100 %. On the 8th day, euthanasia was performed, and four skin flaps and surrounding tissue samples (1.5 × 1 cm) were randomly selected from each group for HE staining, immunohistochemistry, and immunofluorescence staining analysis. All operations were performed under sterile conditions. The animal experiments followed ethical guidelines and were approved by the Institutional Animal Care and Use Committee of the Second Xiangya Hospital, Central South University (Approval No. 20241006).

3.11. Hematoxylin and eosin staining

Sections were deparaffinized in xylene for 30 min and rehydrated in a gradient ethanol series (100 %, 95 %, and 80 %) and distilled water for 5 min. The specimens were soaked in hematoxylin for 5 min and then in PBS for 3 min to reduce background staining. The sections were stained with eosin for 2 min; distilled water for 5 min; 80 %, 90 %, and 100 % ethanol for 5 min; and xylene for 15 min. The slides were mounted and covered with neutral resin. The stained sections were observed and images were captured using a Nikon microscope (Nikon, Tokyo, Japan).

3.12. Immunohistochemical staining (TNF-a and IL-6)

Formalin-fixed and paraffin-embedded tissue sections were deparaffinized, hydrated, antigen-retrieved, washed in PBS, and incubated with 3 % hydrogen peroxide to block endogenous peroxidase activity. After blocking the sections, anti-TNF-a and anti-IL-6 antibodies were added dropwise and incubated overnight at 4 °C. The next day, biotinylated secondary antibody was added and incubated with ABC reagent. DAB was added dropwise for color development, and the reaction was terminated. After hematoxylin staining, dehydration, and mounting, the staining results were observed with a microscope to analyze the expression and distribution of TNF-a and IL-6 in mouse skin flap tissues.

3.13. Statistical analysis

All data were statistically analyzed using IBM SPSS 29.0.1.0 software, and the results were presented as the mean ± standard deviation (SD). Student's t-test was used for comparisons between two groups. For analysis of multiple groups, one-way ANOVA was employed, followed by Tukey's post-hoc test. $P < 0.05$ was considered statistically significant.

4. Discussion and conclusion

Flap surgery, as a cornerstone of reconstructive surgery, has been continuously evolving in terms of its techniques. However, insufficient blood supply and factors related to oxidative stress remain critical determinants for the survival of flaps after surgery [24–26]. Consequently, the use of various drugs with antioxidant, anti-inflammatory, and pro-angiogenic properties holds significant potential for improving flap survival in postoperative care [27]. In this study, quercetin, a natural antioxidant and anti-inflammatory compound, was used to modulate elevated reactive oxygen species (ROS) levels to reduce inflammation, while also promoting the polarization of M2 macrophages, which aids in tissue repair and regeneration. The antioxidant activity of quercetin is achieved through a variety of pathways [28], including activation of the PI3K/Akt signaling pathway, induction of glutathione synthesis, increased expression of endogenous antioxidant enzymes, and regulation of the Nrf2/HO-1 and NF-κB signaling pathways to maintain redox homeostasis. In addition, quercetin reduces the production of inflammatory cytokines, effectively inhibits the overactivation of immune responses, and prevents hepatic ischemia-reperfusion injury by inhibiting inflammation-related signaling pathways, such as NF-κB and AP-1 signaling [29]. HCeO2 is a nanomaterial with a special structure and excellent properties for scavenging oxygen radicals due to the ability to make a fast transition between the two oxidation states Ce^{3+} and Ce^{4+} [30]. The mesoporous structure provides a large specific surface area, which can provide sufficient reaction sites for the photocatalytic reaction and at the same time can make it a promising drug carrier. In this study, quercetin was loaded using HCeO2 and found to exert strong antioxidant, antibacterial and anti-inflammatory effects, which can be useful in skin flap regeneration applications.

Currently, hydrogel research is progressing rapidly and shows great application prospects in the field of regenerative medicine [31,32]. Mao et al. [33] developed a multifunctional dynamically coordinated poly (ethylene glycol) PEG hydrogel loaded with mangiferin liposomes based on Ag-S coordination of four-armed PEG-SH and Ag+ with through development for skin flap regeneration. The hydrogel exhibited excellent drug dispersion and release characteristics for slow and long-lasting drug delivery. Ju et al. [34] on the other hand, developed a natural polysaccharide self-healing hydrogel system for flap regeneration by applying nanozyme in combination with extracellular vesicles. At present, hydrogels show a relatively great research prospect in the field of

flap regeneration, hydrogels can be administered by a single dose, to achieve the localization of the flap continuous drug delivery, reduce the frequency of drug delivery. At the same time, the emergence of some new hydrogels is also expected to play a new role in the field of flap regeneration. For example, conductive hydrogel, there have been studies showing that microcurrent stimulation can accelerate skin wound healing and stimulate blood vessel regeneration, which are of great significance for skin flap regeneration [31,32]. How to realize the translation of hydrogel basic research to clinical application, but also need a lot of research support work, especially the current study is still lack of experimental data of large animal models, rodent experimental results can only illustrate a limited problem.

In short, we developed a quercetin-loaded mesoporous cerium dioxide nanozyme particles double-crosslinked hydrogel (HQu@BC), which promotes macrophage reprogramming and exhibits dual synergistic properties of antimicrobial and antioxidant. We loaded quercetin, which has immunomodulatory properties, into mesoporous cerium dioxide, and our results showed that HQu exerted strong antioxidant and antimicrobial effects, and could effectively scavenge local ROS, protect against mitochondrial damage, anti-inflammatory, bactericidal, and reduce the risk of skin flap necrosis.

CRediT authorship contribution statement

Xiangjun Liu: Writing – review & editing, Writing – original draft, Software, Methodology, Formal analysis, Data curation, Conceptualization. **Yikun Ju:** Writing – review & editing, Visualization, Validation, Supervision, Resources, Formal analysis, Data curation. **Pu Yang:** Visualization, Software, Resources, Formal analysis, Data curation. **Naisi Shen:** Visualization, Validation, Methodology, Data curation. **Yunyuan Shao:** Software, Resources, Methodology. **Anqi Yang:** Visualization, Validation, Resources, Methodology. **Rui Wu:** Validation, Software, Resources, Methodology. **Lanjie Lei:** Writing – review & editing, Supervision, Resources, Project administration, Methodology, Funding acquisition, Conceptualization. **Bairong Fang:** Writing – review & editing, Supervision, Resources, Project administration, Methodology, Funding acquisition, Conceptualization.

Ethics approval and consent to participate

Not applicable.

Funding

This research was supported by the Hunan Provincial Health Commission Scientific Research Project, China (No. C202304106744), the Natural Science Foundation of Hunan Province, China (No. 2024JJ5479, 2021JJ30928), Zhejiang Shuren University Research Project (2023R053 and 2023KJ237), and the Funds of the Natural Science Foundation of Hangzhou(2024SZRYBH180001).

Declaration of competing interest

The authors declare no competing interests.

Acknowledgements

Not applicable.

Appendix A. Supplementary data

Supplementary data to this article can be found online at https://doi.org/10.1016/j.mtbio.2024.101432.

Data availability

Data will be made available on request.

References

[1] A.J. Boulton, L. Vileikyte, G. Ragnarson-Tennvall, J. Apelqvist, The global burden of diabetic foot disease, Lancet 366 (9498) (2005) 1719–1724, https://doi.org/10.1016/s0140-6736(05)67698-2.
[2] M.R. Zeiderman, L.L.Q. Pu, Contemporary reconstruction after complex facial trauma, Burns Trauma 8 (2020) tkaa003, https://doi.org/10.1093/burnst/tkaa003.
[3] A. Yamada, E.S. Chwa, M.J. Boctor, Update on total auricular construction, Plast. Reconstr. Surg. 153 (5) (2024) 1011e–1021e, https://doi.org/10.1097/prs.0000000000011219.
[4] M.L. Candice, S.C. Meredith, Chest complications in autologous breast reconstruction, Plast Aesthet Res 10 (2023) 39, https://doi.org/10.20517/2347-9264.2023.32.
[5] J.C. Dort, D.G. Farwell, M. Findlay, G.F. Huber, P. Kerr, M.A. Shea-Budgell, C. Simon, J. Uppington, D. Zygun, O. Ljungqvist, J. Harris, Optimal perioperative care in major head and neck cancer surgery with free flap reconstruction A consensus review and recommendations from the enhanced recovery after surgery society, JAMA Otolaryngol Head Neck Surg 143 (3) (2017) 292–303, https://doi.org/10.1001/jamaoto.2016.2981.
[6] D.P. Orgill, R. Ogawa, Current methods of burn reconstruction, Plast. Reconstr. Surg. 131 (5) (2013) 827E–836E, https://doi.org/10.1097/PRS.0b013e31828e2138.
[7] A. Stefano, L. Beatrice, V. Daniele, B. Francesco, G. Fortunato, C. Giulia, Treatment of infected soft tissue loss, Plast Aesthet Res 10 (2023) 57, https://doi.org/10.20517/2347-9264.2022.145.
[8] G.B. Grant, C. Yunchan, W. Marcos Lu, C. Karina, M.O. David, Mitigating the impact of skin necrosis in reconstruction after nipple-sparing mastectomy, Plast Aesthet Res 10 (2023) 31, https://doi.org/10.20517/2347-9264.2023.04.
[9] H. Zhou, L. Wang, C. Zhang, J. Hu, J. Chen, W. Du, F. Liu, W. Ren, J. Wang, R. Quan, Feasibility of repairing full-thickness skin defects by iPSC-derived epithelial stem cells seeded on a human acellular amniotic membrane, Stem Cell Res. Ther. 10 (1) (2019) 155, https://doi.org/10.1186/s13287-019-1234-9.
[10] M. Tweel, T. Dow, B. Greene, M. Leblanc, Anatomy, surgical techniques, and clinical outcomes for the medial arm flap: a systematic review, J. Plast. Reconstr. Aesthetic Surg. 92 (2024) 130–144, https://doi.org/10.1016/j.bjps.2024.02.060.
[11] M.V. Schaverien, P. Singh, B.D. Smith, W. Qiao, C.L. Akay, E.S. Bloom, M. Chavez-MacGregor, C.K. Chu, M.W. Clemens, J.S. Colen, R.A. Ehlers, R.F. Hwang, M. M. Joyner, R.D. Largo, A.F. Mericli, M.P. Mitchell, J.W. Shuck, N. Tamirisa, D. Tripathy, M.T. Villa, W.A. Woodward, R. Zacharia, H.M. Kuerer, K.E. Hoffman, Premastectomy radiotherapy and immediate breast reconstruction: a randomized clinical trial, JAMA Netw. Open 7 (4) (2024) e245217, https://doi.org/10.1001/jamanetworkopen.2024.5217.
[12] L.X. Quang, T.N.T. Linh, V.T.H. Ha, L.V.V. Quyen, T.L.H. Ngoc, N.T. Dung, N.T. T. Nga, Y.C. Chen, S.H. Hung, L.H. Dang, A two-flap combination for auricular elevation in microtia reconstruction, Plast. Reconstr. Surg. 151 (6) (2023) 991e–1001e, https://doi.org/10.1097/prs.0000000000010101.
[13] X. Luo, J. Liu, H. Chen, B. Li, Z. Jin, M. Zhao, Y. Xie, C. Yu, X. Zhou, B. Zhao, H. Yan, The feasibility and survival mechanism of a large free flap supported by a novel hybrid perfusion mode, Oral Oncol. 101 (2020) 104506, https://doi.org/10.1016/j.oraloncology.2019.104506.
[14] X. Liu, H. Chen, L. Lei, P. Yang, Y. Ju, X. Fan, B. Fang, Exosomes-carried curcumin based on polysaccharide hydrogel promote flap survival, Int. J. Biol. Macromol. 270 (Pt 1) (2024) 132367, https://doi.org/10.1016/j.ijbiomac.2024.132367.
[15] K. Odake, M. Tsujii, T. Iino, K. Chiba, T. Kataoka, A. Sudo, Febuxostat treatment attenuates oxidative stress and inflammation due to ischemia-reperfusion injury through the necrotic pathway in skin flap of animal model, Free Radic. Biol. Med. 177 (2021) 238–246, https://doi.org/10.1016/j.freeradbiomed.2021.10.033.
[16] W.T. Meng, J. Zhu, Y.C. Wang, C.L. Shao, X.Y. Li, P.P. Lu, M.Y. Huang, F.F. Mou, H. D. Guo, G. Ji, Targeting delivery of miR-146a via IMTP modified milk exosomes exerted cardioprotective effects by inhibiting NF-κB signaling pathway after myocardial ischemia-reperfusion injury, J. Nanobiotechnol. 22 (1) (2024) 382, https://doi.org/10.1186/s12951-024-02631-0.
[17] X. Qu, T. Yang, X. Wang, D. Xu, Y. Yu, J. Li, L. Jiang, Q. Xia, D.G. Farmer, B. Ke, Macrophage RIPK3 triggers inflammation and cell death via the XBP1-Foxo1 axis in liver ischaemia-reperfusion injury, JHEP Rep 5 (11) (2023) 100879, https://doi.org/10.1016/j.jhepr.2023.100879.
[18] S. Andres, S. Pevny, R. Ziegenhagen, N. Bakhiya, B. Schäfer, K.I. Hirsch-Ernst, A. Lampen, Safety aspects of the use of quercetin as a dietary supplement, Mol. Nutr. Food Res. 62 (1) (2018), https://doi.org/10.1002/mnfr.201700447.
[19] S. Tian, J. Mei, L. Zhang, S. Wang, Y. Yuan, J. Li, H. Liu, W. Zhu, D. Xu, Multifunctional hydrogel microneedle patches modulating oxi-inflamm-aging for diabetic wound healing, Small (2024) e2407340, https://doi.org/10.1002/smll.202407340.
[20] C. Yin, X. Qi, J. Wu, C. Guo, X. Wu, Therapeutic contact lenses fabricated by hyaluronic acid and silver incorporated bovine serum albumin porous films for the treatment of alkali-burned corneal wound, Int. J. Biol. Macromol. 184 (2021) 713–720, https://doi.org/10.1016/j.ijbiomac.2021.06.155.
[21] W. Zhang, R. Xu, X. Jin, Y. Wang, L. Hu, T. Zhang, G. Du, Z. Kang, Enzymatic production of chondroitin oligosaccharides and its sulfate derivatives, Front.

Bioeng. Biotechnol. 10 (2022) 951740, https://doi.org/10.3389/fbioe.2022.951740.
[22] O.I. Vernaya, A.N. Ryabev, T.I. Shabatina, D.L. Karlova, A.V. Shabatin, L. N. Bulatnikova, A.M. Semenov, M.Y. Melnikov, V.I. Lozinsky, Cryostructuring of polymeric systems: 62 preparation and characterization of alginate/chondroitin sulfate cryostructurates loaded with antimicrobial substances, Polymers 14 (16) (2022), https://doi.org/10.3390/polym14163271.
[23] K. Duan, N. Mehwish, M. Xu, H. Zhu, J. Hu, M. Lin, L. Yu, B.H. Lee, Autoclavable albumin-based cryogels with uncompromising properties, Gels 9 (9) (2023), https://doi.org/10.3390/gels9090712.
[24] X. Zhu, G. Yu, Y. Lv, N. Yang, Y. Zhao, F. Li, J. Zhao, Z. Chen, Y. Lai, L. Chen, X. Wang, J. Xiao, Y. Cai, Y. Feng, J. Ding, W. Gao, K. Zhou, H. Xu, Neuregulin-1, a member of the epidermal growth factor family, mitigates STING-mediated pyroptosis and necroptosis in ischaemic flaps, Burns Trauma 12 (2024), https://doi.org/10.1093/burnst/tkae035 tkae035.
[25] G. Yu, J. Ding, N. Yang, L. Ge, N. Chen, X. Zhang, Q. Wang, X. Liu, X. Zhang, X. Jiang, Y. Geng, C. Zhang, J. Pan, X. Wang, W. Gao, Z. Li, H. Zhang, W. Ni, J. Xiao, K. Zhou, L. Yang, Evaluating the pro-survival potential of apoptotic bodies derived from 2D- and 3D- cultured adipose stem cells in ischaemic flaps, J. Nanobiotechnol. 22 (1) (2024) 333, https://doi.org/10.1186/s12951-024-02533-1.
[26] J. Lou, X. Wang, H. Zhang, G. Yu, J. Ding, X. Zhu, Y. Li, Y. Wu, H. Xu, H. Xu, W. Gao, J. Xiao, K. Zhou, Inhibition of PLA2G4E/cPLA2 promotes survival of random skin flaps by alleviating Lysosomal membrane permeabilization-Induced necroptosis, Autophagy 18 (8) (2022) 1841–1863, https://doi.org/10.1080/15548627.2021.2002109.
[27] G. Yu, Y. Chen, N. Yang, H. Zhang, X. Zhang, Y. Geng, J. Zhao, Z. Chen, C. Dong, L. Lin, J. Qi, X. Zhang, X. Jiang, W. Gao, Y. Cai, X. Wang, J. Ding, J. Xiao, K. Zhou, Apoptotic bodies derived from fibroblast-like cells in subcutaneous connective tissue inhibit ferroptosis in ischaemic flaps via the miR-339-5p/KEAP1/nrf2 Axis, Adv. Sci. 11 (24) (2024) e2307238, https://doi.org/10.1002/advs.202307238.
[28] H. Zou, H. Ye, R. Kamaraj, T. Zhang, J. Zhang, P. Pavek, A review on pharmacological activities and synergistic effect of quercetin with small molecule agents, Phytomedicine 92 (2021) 153736, https://doi.org/10.1016/j.phymed.2021.153736.
[29] J. Lin, F. Li, J. Jiao, Y. Qian, M. Xu, F. Wang, X. Sun, T. Zhou, H. Wu, X. Kong, Quercetin, a natural flavonoid, protects against hepatic ischemia-reperfusion injury via inhibiting Caspase-8/ASC dependent macrophage pyroptosis, J. Adv. Res. (2024), https://doi.org/10.1016/j.jare.2024.05.010.
[30] H. Nosrati, M. Heydari, M. Khodaei, Cerium oxide nanoparticles: synthesis methods and applications in wound healing, Mater. Today Bio 23 (2023), https://doi.org/10.1016/j.mtbio.2023.100823.
[31] W. Li, X. Yang, P. Lai, L. Shang, Bio-inspired adhesive hydrogel for biomedicine—principles and design strategies, Smart Medicine 1 (1) (2022) e20220024, https://doi.org/10.1002/SMMD.20220024.
[32] Y. Wang, J. Guo, X. Cao, Y. Zhao, Developing conductive hydrogels for biomedical applications, Smart Medicine 3 (1) (2024) e20230023, https://doi.org/10.1002/SMMD.20230023.
[33] X. Mao, R. Cheng, H. Zhang, J. Bae, L. Cheng, L. Zhang, L. Deng, W. Cui, Y. Zhang, H.A. Santos, X. Sun, Self-healing and injectable hydrogel for matching skin flap regeneration, Adv. Sci. 6 (3) (2018), https://doi.org/10.1002/advs.201801555.
[34] Y. Ju, P. Yang, X. Liu, Z. Qiao, N. Shen, L. Lei, B. Fang, Microenvironment remodeling self-healing hydrogel for promoting flap survival, Biomater. Res. 28 (2024), https://doi.org/10.34133/bmr.0001.